https://doi.org/10.5194/egusphere-2026-3473
Preprint. Discussion started: 21 July 2026

Loess Soil Structural Changes Induced by Bio- and Synthetic Polymer Stabilizers: Geoelectrical Insights

Sonya Sara Altzitser [1], Yael Golda Mishael [1], Nimrod Schwartz [1]

[1] Department of Soil and Water Sciences, The Robert H. Smith Faculty of Agriculture, Food and Environment, The Hebrew University of Jerusalem, Rehovot, 7610001, Israel

Correspondence to: Nimrod Schwartz (Nimrod.schwartz@mail.huji.ac.il)

Abstract. Traditional assessments of soil aggregate stability rely on destructive, ex situ protocols that fail to capture the continuous evolution of soil architecture. This study evaluates the divergent stabilization trajectories induced by chia seed mucilage (CSM) and anionic polyacrylamide (A-PAM) in loess soil over a 20-day incubation. By integrating Spectral Induced Polarization (SIP) with microbial respiration and tracer breakthrough experiments, we track the transition from initial aggregation to long-term structural outcomes. Results demonstrate that CSM-induced stabilization is strictly transient; rapid microbial degradation of the biopolymer results in progressive reversal of the induced structural modifications and a reversion to baseline hydraulic behaviour. In contrast, A-PAM provides persistent physicochemical reinforcement, establishing a dual-porosity regime characterized by immobile water domains and preferential flow pathways. SIP signatures effectively resolved these dynamics: high-frequency shifts in quadrature conductivity (σ'') provided geoelectrical evidence of micro-aggregate formation, while the development of a 'conductive reservoir' in in-phase conductivity (σ') identified hydraulically isolated ion accumulation. These findings establish SIP as a high-resolution, non-invasive proxy for monitoring the interplay between biochemical persistence and the mechanical stabilization of soil structure.

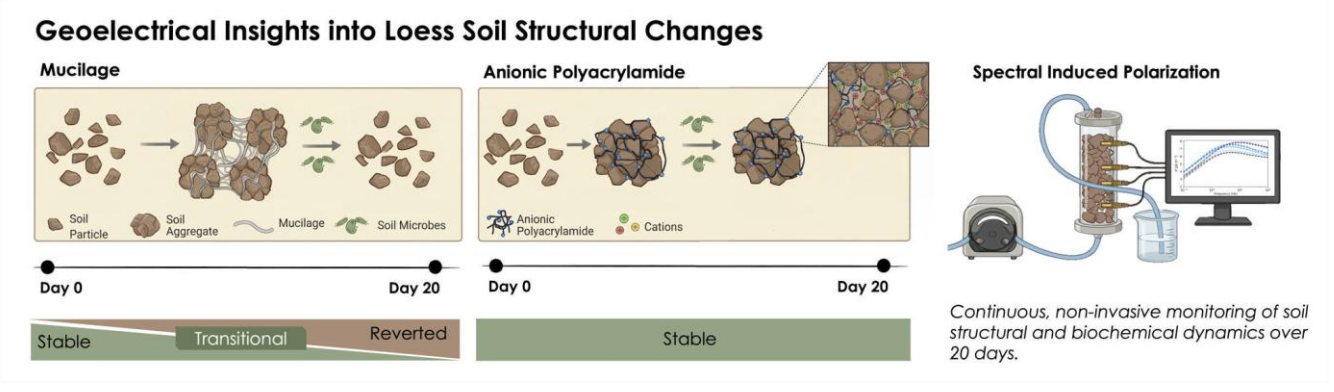

https://doi.org/10.5194/egusphere-2026-3473
Preprint. Discussion started: 21 July 2026

1. Introduction

Soil erosion and thereby degradation of soil physical quality are key constraints on global agricultural productivity and ecosystem functionality (Pimentel and Kounang, 1998; Wuepper et al., 2019; Pandey et al., 2021; Borrelli et al., 2021; Zhang et al., 2025). Erosion involves the detachment and transport of soil particles by water and wind, processes that are largely controlled by the soil's resistance to mechanical stress. Consequently, soil susceptibility to erosion is intrinsically linked to soil structure, which is governed by the formation and persistence of aggregates. These aggregates emerge from the rearrangement, flocculation, and cementation of primary particles by organic matter, carbonates, oxides, and biological exudates. Therefore, aggregate stability serves as a key indicator of soil structural integrity (Lal, 2001; Bronick and Lal, 2005; Alletto et al., 2010; Ball, 2013; Rabot et al., 2018; Rinot et al., 2019; Tully and McAskill, 2020; Shahane and Shivay, 2021).

To mitigate erosion and stabilize soil structure, numerous soil stabilizers have been tested for agriculture and engineering purposes. Among them, synthetic organic polymers are particularly effective, as they enhance aggregate stability, reduce clay dispersion, and strengthen cohesion between soil particles (Lee et al., 2013; Mamedov et al., 2020; Almajed et al., 2022). The most widely used synthetic organic polymer in soil stabilization is anionic polyacrylamide (A-PAM), due to its non-toxic nature and physicochemical properties (Seybold, 1994). Mamedov et al. (2010) demonstrated that A-PAM stabilizes existing aggregates and improves inter-particle bonding, particularly in soils with low stability or low organic carbon content. Albalasmeh et al. (2021) reported that low-molecular-weight A-PAM could enhance soil aggregate stability threefold compared to untreated soils, while Soltani et al. (2022) found that the application of an optimal dosage (0.2 g L^{-1}) effectively minimizes soil swelling and shrinkage, whereas higher doses were less beneficial. Together, these findings highlight the consistent effectiveness of A-PAM as a soil stabilizer.

In addition to synthetic polymers, natural stabilizers (biopolymers) have also been explored. Examples include polysaccharides, composts, and biochar, which can enhance aggregation and soil porosity (Huang et al., 2021). Mamedov et al. (2010) showed how various polysaccharides, such as xanthan gum, guar gum, and carboxymethyl cellulose, enhance soil stability by increasing viscosity, aggregation, adsorption, and cross-linking bond formation, resulting in improved erosion stability. Likewise, Bozyigit et al. (2023) demonstrated that eco-friendly polymers, such as guar gum, improve soil stability by enhancing strength properties and reducing freeze-thaw disaggregation.

A well-known natural stabilizer in the rhizosphere is mucilage, a gelatinous root exudate composed of high-molecular-weight substances, mainly polysaccharides. However, despite its established role in promoting particle adhesion and influencing soil-microbe interactions, comparative studies investigating its efficacy against synthetic benchmarks, such as A-PAM, remain scarce. Previous research has shown that the addition of mucilage induced an immediate and significant increase in aggregate stability relative to untreated soils (Traoré et al., 2000; Marsico et al., 2018; Brax et al., 2020; Zhong et al., 2021).

Soil aggregate stability is predominantly assessed ex situ on disturbed samples, a practice that may obscure the complex in-field dynamics of aggregation and disaggregation. Traditional protocols rely heavily on wet sieving techniques, which quantify

https://doi.org/10.5194/egusphere-2026-3473
Preprint. Discussion started: 21 July 2026

the mass of stable aggregates surviving water immersion and mechanical oscillation (Yoder, 1936; Kemper and Rosenau, 1986). To improve sensitivity and capture specific breakdown mechanisms, such as slaking or mechanical breakdown, more advanced approaches have been introduced. These include protocols distinguishing between wetting conditions (Le Bissonnais, 1996) and the Aggregate Durability Index (ADI), which utilizes laser diffraction to precisely characterize the kinetics of fragment size distribution (Dor et al., 2019). However, regardless of their sophistication, these methods remain inherently destructive and retrospective, failing to capture the continuous structural evolution of soil in real-time (Garland et al., 2024).

In situ monitoring of structural changes and their coupling to soil chemistry offers critical insights that complement traditional ex situ methods. Geoelectrical techniques, such as Spectral Induced Polarization (SIP), hold potential for such non-invasive assessment due to their intrinsic sensitivity to soil pore geometry, fluid distribution, and surface properties. Previous research has successfully employed electrical measurements to characterize fundamental particle properties, soil-organic matter interactions, and geochemical processes at the grain-fluid interface (Vinegar and Waxman, 1984; Vaudelet et al., 2011; Schwartz et al., 2012; Schwartz and Furman, 2012; Kessouri et al., 2019; Mellage et al., 2022; Altzitser et al., 2025). Since these physicochemical mechanisms intrinsically drive the stabilization of soil structure (Yudina and Kuzyakov, 2023), we hypothesize that SIP can serve as a sensitive proxy for detecting micro-structural changes induced by polymer stabilizers.

SIP involves applying a low-frequency, time-dependent electrical field and recording the resulting potential. This technique captures both the conductive (energy dissipation) and capacitive (energy storage) characteristics of the medium, characterized by the in-phase (σ') and quadrature (σ'') conductivity components, respectively. σ' receives contributions from pore-water conductivity (σ'_w), scaled by the formation factor (F), a geometric parameter describing the tortuosity of current pathways, and from surface conductance (σ'_s) along mineral interfaces. σ'', is directly associated with the interfacial chemistry of the grain surface and polarization processes at the electrical double layer (EDL), and is frequency dependent (Binley and Kemna, 2005; Binley and Slater, 2020; Reynolds, 2011).

Consequently, this study evaluates and compares the efficacy of chia seed mucilage (CSM) and A-PAM (a synthetic benchmark) in stabilizing loess soil. While the stabilizing properties of mucilage are established in the context of natural rhizospheric exudates, this work investigates the application of CSM as a deliberate soil stabilizer, comparing its functional capacity with established synthetic polymers. A dual approach was implemented, integrating standard ex situ analyses of microbial activity and aggregate stability with continuous in situ SIP monitoring of soil columns over a 20-day period. Concentration levels were set at 0.035% (w/w) to represent typical environmental concentrations in the natural rhizosphere, and 0.175% (w/w) to assess whether increased amendment mass can improve structural durability over time. The study hypothesizes that while both polymers induce initial aggregation, their stabilization trajectories will diverge based on the biochemical persistence of the synthetic polymer versus the rapid microbial degradation of the natural mucilage. These structural and biochemical transformations are posited to yield distinct spectral electrical signatures, thereby testing the applicability of SIP as a high-resolution, real-time proxy for soil stabilization dynamics.

https://doi.org/10.5194/egusphere-2026-3473
Preprint. Discussion started: 21 July 2026

2. Materials and Methods

To investigate how natural and synthetic polymer stabilizers influence soil structure over time, column experiments were conducted with control, mucilage, anionic polyacrylamide (A-PAM), and nonionic polyacrylamide (N-PAM) treatments at different concentrations, monitored over a 20-day period. N-PAM was included as an electrochemically neutral reference. This treatment allowed for the differentiation between the geoelectrical impacts of neutral polymer adsorption and the charge-dependent interactions associated with A-PAM and CSM. SIP measurements captured changes in in-phase and quadrature conductivity, while effluent chemical analyses provided insight into solution composition and mineral dissolution. Aggregate stability tests and conservative tracer breakthrough experiments were conducted to evaluate structural evolution under various treatments.

2.1 Materials

Loess soil (sandy clay loam) was collected from 0-20 cm depth from an uncultivated site in Mishmar Hanegev, Israel. Chia seeds were purchased from a local supermarket. Calcium chloride, potassium iodide, nonionic polyacrylamide (N-PAM) of 30% hydrolysis, sodium hexametaphosphate 65-70% P_2O_5, and phenolphthalein were purchased from Sigma-Aldrich. An anionic polyacrylamide (A-PAM) of high molecular weight (≈18×10^6 Da) and 30% hydrolysis with a trade name of Superfloc A-110 was purchased from Kemira, GA, USA.

2.2 Methods

2.2.1 Extraction of Chia Seed Mucilage

Mucilage was extracted from chia seeds (Salvia hispanica L.) and used as an analog for rhizosphere mucilage, as its chemical composition is comparable to maize root exudates (Carminati and Vetterlein, 2013; Kroener et al., 2014). The extraction procedure followed the protocol described by Capitani et al. (2013). Briefly, the chia seeds were immersed in deionized water at a 1:10 ratio and maintained at 27°C for 4 h. The resulting mucilage suspension was freeze-dried and passed through an 800 µm sieve to obtain the final powder.

2.2.2 Soil Preparation

Untreated loess soil served as the control, and six amended treatments were prepared: low and high concentrations of mucilage (ML and MH, respectively), non-ionic polyacrylamide (N-PAML and N-PAMH, respectively), and anionic PAM (A-PAML and A-PAMH, respectively). N-PAM was utilized exclusively in the SIP column experiments as a non-ionic reference to differentiate between the geoelectrical impacts of neutral polymer adsorption and the charge-dependent interactions associated with A-PAM, and CSM. Air-dried soil was sieved to <2 mm and then amended with either 0.035% or 0.175% (w/w) of the

https://doi.org/10.5194/egusphere-2026-3473
Preprint. Discussion started: 21 July 2026

mucilage or PAM for the low and high treatments, respectively. The polymers were first dissolved in 5 mM $CaCl_2$ solution and then mixed with the soil to achieve uniform wetting of 10% (w/w), ensuring consistent polymer distribution. The treated soils were thoroughly homogenized and air-dried at room temperature for 24 h before use. The control soil underwent the same procedure but was wetted with a polymer-free 5 mM $CaCl_2$ solution.

2.2.3 Measurement of Microbial CO_2 Emission

Microbial respiration was evaluated in five treatments: control, ML, MH, A-PAML, and A-PAMH. Soils were prepared as described above. For each treatment, air-dried soil was mixed with 30% (w/w) of 5 mM $CaCl_2$ solution to achieve uniform moisture. A total of 65.7 ± 1.65 g of wet soil was placed into 50 mL wide-neck glass jars, which were sealed inside an airtight, rubber-sealed container along with an open vial containing 2 mL of 1 M NaOH to trap CO_2. The incubation was conducted at 25 °C in the dark. NaOH traps were destructively sampled on days 1, 3, 4, 10, 14, 17, and 20 of the experiment. The trapped CO_2 was quantified by titration with 0.2 M HCl using phenolphthalein as a visual pH indicator. Blank containers containing only NaOH were used for the background correction. CO_2 emission rates were calculated based on the acid volume required for neutralization, and the results were expressed in mg CO_2 kg^{-1} day^{-1}, normalized to soil dry weight and incubation time (Bartha and Pramer, 1965).

2.2.4 Wet-Sieving Aggregate Stability

To quantify the resistance of soil aggregates to slaking and physicochemical dispersion, aggregate stability was assessed for five treatments: control, ML, MH, A-PAML, and A-PAMH, using a wet sieving apparatus (Eijkelkamp, M-0813E). Soils were prepared as described in Section 2.2.2, saturated with 30% (w/w) 5 mM $CaCl_2$, and sealed. For each measurement (days 1, 7, 20), samples were unsealed 24 h prior and air-dried at 25 °C. Aggregates <2 mm were collected by sieving, and 4 g subsamples were weighed into 60-mesh sieves for analysis. To minimize slaking during immersion, the aggregates were lightly pre-moistened using a fine mist and rested for 5-10 min. Sieves were then oscillated in distilled water for 3 min (1.3 cm stroke at 34 cycles min^{-1}), followed by dispersion in 2 g L^{-1} sodium hexametaphosphate solution until complete breakdown of the aggregates. Following agitation, the material was separated into three fractions based on operational stability degree and oven-dried at 110 °C: (i) particles that passed the sieve during the initial water treatment (least stable fraction), (ii) particles that passed after chemical dispersion (intermediately stable fraction), and (iii) particles retained on the sieve after full dispersion (sand and highly stable aggregates). The sand fraction was estimated from control samples, in which no highly stable aggregates were expected, and was subtracted from all treatments to isolate the truly stable particulate mass. The relative mass of each fraction was used to estimate the distribution of the aggregate stability within each treatment and time point.

https://doi.org/10.5194/egusphere-2026-3473
Preprint. Discussion started: 21 July 2026

2.2.5 Iodide Tracer for Structural Assessment

To assess soil structure variations among treatments, iodide (introduced as KI) breakthrough experiments were conducted immediately after column packing (day 0) and after 20 days of incubation. Iodide (I^-) was selected as an inert tracer with negligible soil adsorption, allowing its breakthrough behavior to reflect the differences in pore connectivity and hydraulic properties between treatments. Experiments were performed in triplicate for three treatments: control, ML, and A-PAML, using the same SIP columns described in Section 2.2.6. A-PAMH treatment was not included because a stable flow could not be maintained owing to excessive backpressure and leakages. After the initial 3 PV flushing with 5 mM $CaCl_2$, the inlet solution was switched to 55 mM KI in 5 mM $CaCl_2$, and flow was continued until approximately 3.5 PVs were eluted. Effluent samples of 20 mL were collected every 40 min and immediately analyzed for iodide concentration using an iodide-selective electrode (HI-4111, Hanna Instruments, Cambridge, UK), along with pH and EC. Breakthrough curves (C/C_0 vs. PV) were constructed to assess tracer transport and infer structural differences among treatments.

The transport of iodide through the saturated columns was modeled using the one-dimensional Advection-Dispersion Equation (ADE):

$$\frac{\partial C}{\partial t} = D\frac{\partial^2 C}{\partial x^2} - v\frac{\partial C}{\partial x} \quad (1)$$

where C $[mM\ L^{-3}]$ is the concentration, t $[min]$ is time, x $[cm]$ is the distance, and $\bar{v}$ $[cm\ min^{-1}]$ is the average pore-water velocity. The hydrodynamic dispersion coefficient, D $[cm^2\ min^{-1}]$, incorporates the effects of mechanical dispersion and molecular diffusion. To justify the assumption that transport was governed by mechanical dispersion, the Péclet number ($Pe = vL/D_s$) was evaluated. Using the experimental pore-water velocity ($v = 0.162\ cm\ min^{-1}$), a characteristic length ($L \cong 0.0015cm$) based on the average particle radius of the loess (Pye, 1984), and an effective diffusion coefficient ($D_s = 6.12 \cdot 10^{-5}\ cm^2\ min^{-1}$) for a confined silt-clay mixture (Ayral-Cinar and Demond, 2017), Pe was determined to be ≈ 4, which indicates that under the experimental conditions the transport is dominated by mechanical dispersion. The dispersion coefficient was therefore defined as:

$$D = \alpha v \quad (2)$$

where α $[cm]$ represents the longitudinal dispersivity, a characteristic property of the porous medium geometry. To accurately represent the experimental step-input injection, the model was constrained by the following initial and boundary conditions:

$$C(x, 0) = 0 \qquad x \geq 0 \quad (3a)$$

$$\left(vC - D\frac{\partial C}{\partial x}\right)\Big|_{x=0} = vC_0 \qquad t > 0 \quad (3b)$$

https://doi.org/10.5194/egusphere-2026-3473
Preprint. Discussion started: 21 July 2026

(3c) $$\frac{\partial C}{\partial x}(\infty, t) = 0 \qquad t \geq 0$$

The third-type (Cauchy) inlet boundary condition (Eq. 3b) was selected to ensure mass flux continuity at the injection point. The analytical solution for these conditions is given by Van Genuchten and Alves (1982). Transport parameters were estimated by inverse fitting of the analytical solution to the experimental breakthrough curves using a custom-made Python script. In this analysis, the water content (θ) was constrained to the experimentally calculated porosity ($\phi = 0.41 - 0.45$), reflecting the saturated state of the columns.

2.2.6 Spectral Induced Polarization Measurements

SIP measurements were used to evaluate variations in bulk and surface conductivity following the application of control, mucilage, N-PAM, and A-PAM treatments. Signals were acquired using a PSIP impedance spectrometer (Ontash & Ermac Inc, NJ, USA) in polyvinyl chloride (3 cm diameter, 30 cm long) columns. Each column was equipped with a four-electrode array consisting of 6 mm diameter brass electrodes (Fig. 1). The current injection electrodes (8 cm long) crossed the entire sample cross-section, while the potential electrodes (5 cm long) were recessed into the electrode hole to minimize electrode polarization effects (as in Schwartz and Furman, 2012). Electrical contact between the potential electrodes and the sample was ensured through the electrolyte solution. The geometric factor (G) was determined by measuring the impedance of a series of electrolytes with different electrical conductivities. Before the experiments, the setup was tested with 5 mM $CaCl_2$, and the measured phase remained below 1 mrad up to 1 kHz, confirming minimal polarization of the sample holder.

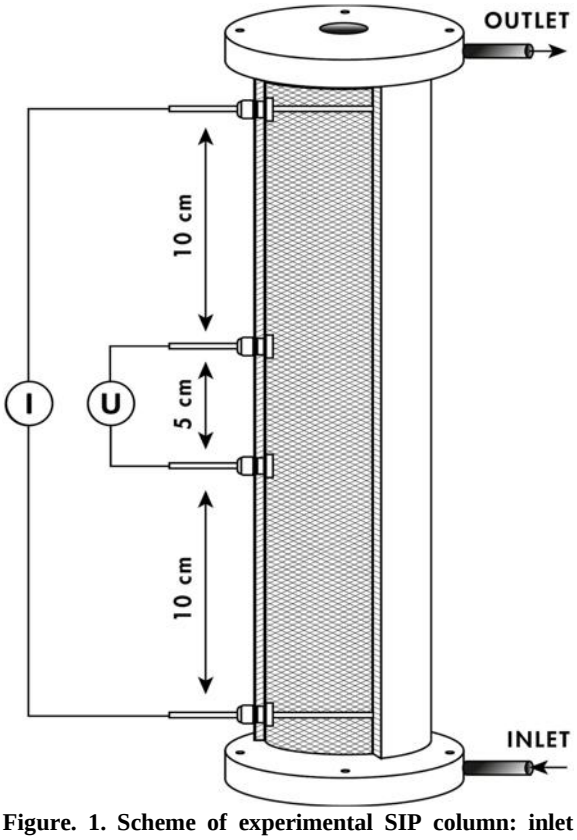

Figure. 1. Scheme of experimental SIP column: inlet solution is injected in through the bottom and the outlet is collected in fractions. The current (I) is injected between the top and the bottom electrodes, and the SIP signal is measured between the potential electrodes (U)

2.2.7 SIP Columns Experiments

SIP signatures were collected over a 20 days periods for six treatments: control, ML, MH, N-PAML, N-PAMH, and A-PAML. A-PAMH treatment was not included because stable flow could not be achieved owing to excessive backpressure and leakage. Air-dried soils, prepared as described in section 2.2.2, were packed into vertical SIP columns in ~50 mL increments, with gentle compression after each addition. Based on a particle density of 2.65 g cm^{-3} (Warrick, 2002), the columns exhibited porosities ranging from 0.41 to 0.45, with an overall standard

https://doi.org/10.5194/egusphere-2026-3473
Preprint. Discussion started: 21 July 2026

deviation of ±0.01 across treatments. After packing, the columns were saturated from the bottom with 5 mM $CaCl_2$ to displace air and leach soluble salts. Saturated flow was maintained using a peristaltic pump (Masterflex L/S series, Cole-Parmer, IL, USA) at 0.5 mL min^{-1} for three pore volumes (PV). The effluent electrical conductivity (EC) stabilized at 1370–1760 µS cm^{-1} after this flushing period. The final 20 mL of the flushing solution was collected at both day 0 and 20, and analyzed for soluble cations concentrations by ICP-AES (Arcos, Spectro Ltd., Germany).

3. Results

3.1 CO_2 Emission Rates

To evaluate the effect of polymer type and concentration on microbial activity, CO_2 emission rates were measured in loess soil subjected to five treatments: control (untreated), low and high mucilage (ML, MH), and low and high anionic PAM (A-PAML, A-PAMH) (Fig. 2). CO_2 emission may also be attributed to abiotic reactions; therefore, we address the differences between treatments rather than absolute values. For all treatments, CO_2 emissions increased between days 1 and 14, followed by a decrease. Specifically, CO_2 emission rates for the MH treatment were significantly higher ($P < 0.05$) than all other treatments on days 3 and 7, representing a 3-fold increase relative to the other treatments. A-PAM treatments (high and low concentrations) produced the lowest CO_2 emissions throughout incubation and did not differ statistically from one another. By day 20, CO_2 emissions across all treatments declined to similar rates, yet higher than the initial values.

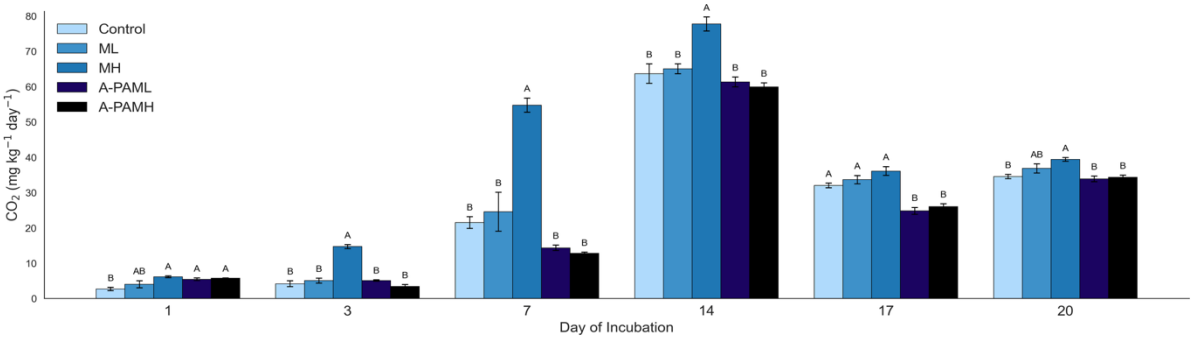

Figure. 2. Effect of polymer stabilizers on CO_2 emission (mg CO_2 kg^{-1} day^{-1}) ± SD (n=4) during a 20-day incubation period. Treatments include control (untreated soil), low and high mucilage (ML, MH), and low and high anionic PAM (A-PAML, A-PAMH). Different capital letters indicate significant differences among treatments within each day (P < 0.05).

3.2 Soil Aggregate Stability

Soil stability changes in response to mucilage and A-PAM treatments were assessed by the wet sieving method. The distribution of aggregates across stability degrees (low, medium, high) diverged strongly between treatments over 20 days

https://doi.org/10.5194/egusphere-2026-3473
Preprint. Discussion started: 21 July 2026

(Fig. 3). Soil aggregate stability for the control treatment, remained low throughout the entire experiment. At day one, soil aggregate stability for the mucilage treatments increased, with ~50% aggregates classified as medium stability, in comparison to the control. At day seven, soil aggregate stability for the mucilage treatments differed, with a decrease in stability for the ML and an increase for MH. By day twenty, soil aggregate stability for both mucilage treatments had decreased compared to day 1 and 7. By day seven and throughout the remainder of the experiment, soil aggregate stability for the A-PAM treatments was notably higher than the control and mucilage treatments.

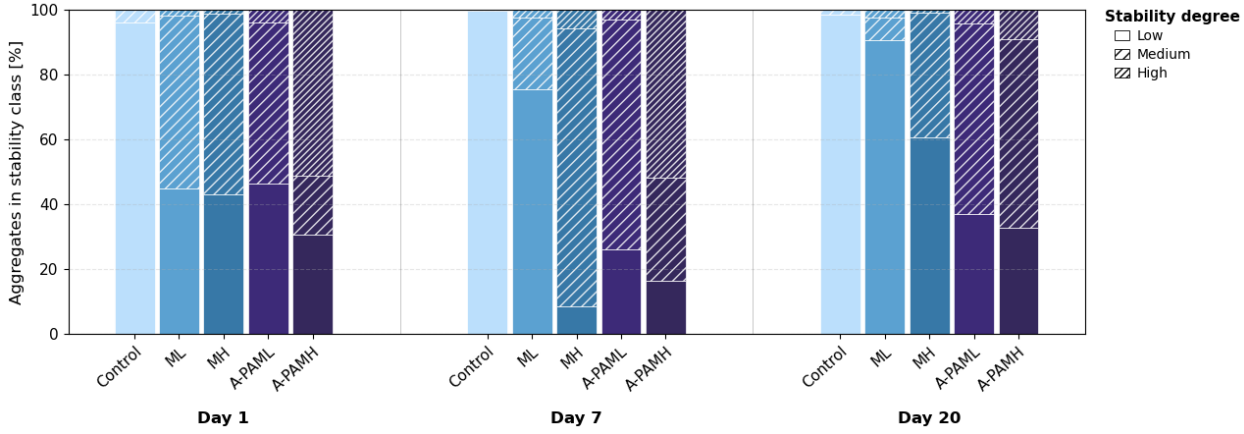

Figure. 3. Normalized distribution of soil aggregates across stability degree (low, medium, high) in soil treated with control, mucilage (ML, MH), and anionic PAM (A-PAML, A-PAMH). Values represent the mean fraction of aggregates measured at three sampling times (Day 1, 7, and 20) during the 20-day incubation.

3.3 Soil Structural Changes: Reflected by KI Breakthrough

Iodide breakthrough experiments were performed to trace the structural changes induced by ML and A-PAML treatments, with iodide serving as an inert tracer reflecting their effects on solute transport through the soil. The resulting experimental breakthrough curves and their corresponding fits to the ADE (Eq. 1) are presented in Fig. 4 for day 0 and day 20. At day 0 (Fig. 4a), the control and ML treatments exhibited classical sigmoidal breakthrough curves that fitted well to the standard ADE model. The ML treatment displayed higher dispersivity ($\alpha = 1.47\ cm$) compared to the control ($\alpha = 0.55\ cm$) and a slight delay in reaching complete saturation ($C/C_0 = 1$). In contrast, despite intermediate dispersivity ($\alpha = 1.21\ cm$), A-PAML treatment displayed pronounced tailing with a less accurate fit to the ADE model, which notably deviated from the experimental data, failing to fully capture the observed tail.

By day 20 (Fig. 4b), the control breakthrough behaviour remained comparable to day 0 ($\alpha = 1.16\ cm$). Notably, the ML treatment shifted to closely resemble the control profile ($\alpha = 1.33\ cm$). In sharp contrast, the A-PAML treatment exhibited a significant transformation relative to day 0, displaying extensive tailing and a marked increase in fitted dispersivity ($\alpha = 3.78\ cm$). While the goodness of fit decreased for all treatments compared to day 0, the standard ADE model specifically failed to capture the prolonged tail observed in the A-PAML treatment. For the control and ML treatments, the analytical

https://doi.org/10.5194/egusphere-2026-3473
Preprint. Discussion started: 21 July 2026

solution remained centered on the experimental data points throughout the breakthrough. Conversely, the A-PAML fit exhibited a systematic deviation, overpredicting concentrations during the initial rise (PV 0.7–1.2) and underpredicting the measured values during the extended tailing phase (PV > 1.5).

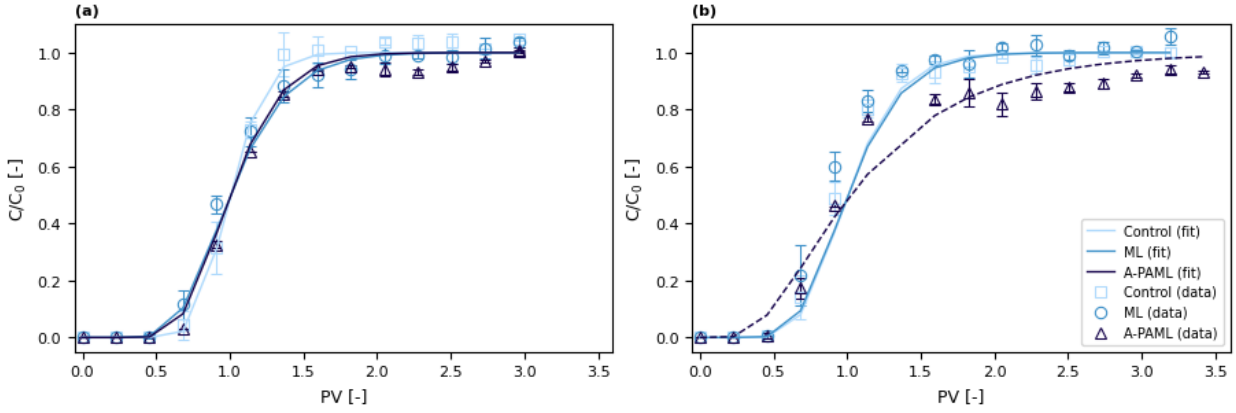

Figure. 4. Breakthrough curves of KI tracer in soil columns under control, ML, and A-PAM treatments at (a) day 0 and (b) day 20. Symbols denote measured values and lines represent standard ADE model fits. At day 20, the A-PAM treatment shows a noticeably poorer agreement with the model, indicating a deviation from ideal tracer transport behaviour.

3.4 Temporal SIP Signatures

SIP monitoring was conducted for the control, ML, MH, A-PAML, N-PAML, and N-PAMH column treatments during 20 days of incubation (Fig. 5). SIP signatures revealed treatment-dependent differences in the in-phase conductivity (σ'), which reflects pore-water electrolyte conductivity and surface conduction, and in the quadrature conductivity (σ''), which is associated with interfacial polarization. For σ' (Fig. 5a), all treatments showed an initial rise during the first 8 days, which was most pronounced in MH and A-PAML (60% and 72% increase, respectively), while the control and ML exhibited a more moderate increase. Thereafter, the rise in σ' became gradual across treatments. By day 20, σ' had risen across treatments, with MH and A-PAML showing the most pronounced increases (80% and 86% above initial values, respectively), whereas the control and ML reached more moderate levels of 50% and 60%, respectively. In contrast, both N-PAM treatments showed a slower initial increase in σ' during the first 7 days, which became more pronounced thereafter, resulting in a total rise of approximately 47% by day 20, comparable to the control.

σ'' (Fig. 5b) values declined during the first week in all treatments except N-PAM, after which they stabilized. MH, and A-PAML showed the steepest decline of about 25% in the first week, while control and ML followed similar trend but with more gradual slopes (21% and 17%, respectively). From day 7 to day 20, control and A-PAML showed slowed decrease of ~10%, while both mucilage treatments remained constant. Overall, A-PAML exhibited the steepest decrease in σ'' of 35% from its initial value. By contrast, both N-PAM treatments showed only minor decreases of 7%, with values remaining nearly constant throughout the entire experiment.

https://doi.org/10.5194/egusphere-2026-3473
Preprint. Discussion started: 21 July 2026

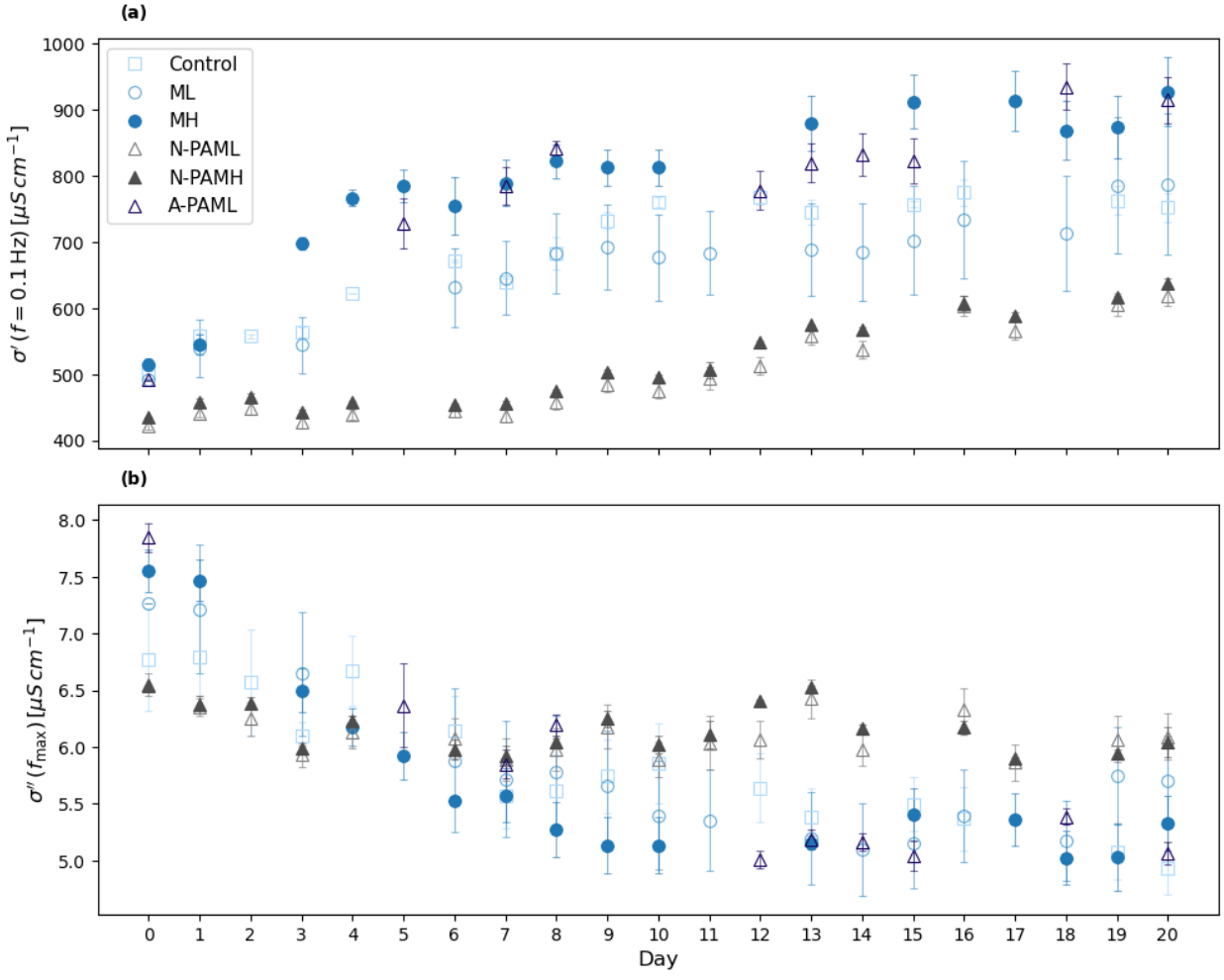

Figure 5. Temporal evolution of SIP parameters in polymer-treated soils. (a) In-phase conductivity (σ') measured at 0.1 Hz, (b) Quadrature conductivity (σ'') at the peak frequency, as a function of incubation time. Symbols represent mean values of replicate columns for each treatment (Control, ML, MH, N-PAML, N-PAMH, A-PAML)

3.5 SIP Spectra Day 0 vs. Day 20

The σ' and σ'' spectral signatures for the control, ML, MH, A-PAML, N-PAML, and N-PAMH treated soils at days 0 and 20 are shown in Fig. 6. For σ' (Fig. 6a) all treatments except N-PAM exhibited similar σ' values, ranging between 491 and 514 µS cm^{-1}. In contrast, both N-PAM treatments showed lower values of 422-434 µS cm^{-1}, approximately 16% lower than the other treatments. The EC of the inlet solution (5mM $CaCl_2$) was 1000 µS cm^{-1}, while effluent EC stabilized at 1370 - 1760 µS cm^{-1} after 3 PVs. After 20 days of incubation, σ' (Fig. 6c) increased substantially across all treatments. MH and A-PAML showed the highest values of approximately 920 µS cm^{-1}, representing increases of 80-86% from initial values of σ'. control and ML treatments displayed more gradual increases of 50-60%, reaching intermediate σ' of 750-780 µS cm^{-1}. Both

https://doi.org/10.5194/egusphere-2026-3473
Preprint. Discussion started: 21 July 2026

N-PAM treatments remained lower at σ' of 620-640 µS cm^{-1}, though these values still represented a 47% increase from day 0.

The highest σ'' at peak frequency was observed for A-PAML, MH and ML treatments, with similar peak values of 7.263 – 7.844 µS cm^{-1} (Fig. 6b). The control and both N-PAM treatments displayed lower σ'' responses, 16-22% below the highest values. The peak frequency was similar among all treatments (~4–5.5 Hz) except A-PAML, which shifted toward higher frequencies (8.89 Hz). By day 20, σ'' values decreased across all treatments, with peak values converging to 5-6 µS cm^{-1} regardless of treatment (Fig. 6d). The spectra became considerably flatter for all treatments, making identification of a distinct peak frequency more challenging. Despite this convergence, A-PAML maintained a noticeably different spectral shape compared to the other treatments.

In addition to the SIP measurement soil solution samples (20 mL) were collected from all treatments at day 0 and day 20 for determination of soluble cation concentrations. The treatments differed in their temporal trends and magnitudes, yet in all cases Ca^{2+} remained the dominant cation (Fig. 7). While all treatments exhibited similar Ca^{2+} levels at day 0, pronounced differences developed by day 20. The control and mucilage treated soils (ML and MH) showed a 3-3.5 fold rise in both Ca^{2+} and total cation concentrations, compared with only a two-fold increase under A-PAM and almost no change under N-PAM (Fig. 7a, b).

https://doi.org/10.5194/egusphere-2026-3473
Preprint. Discussion started: 21 July 2026

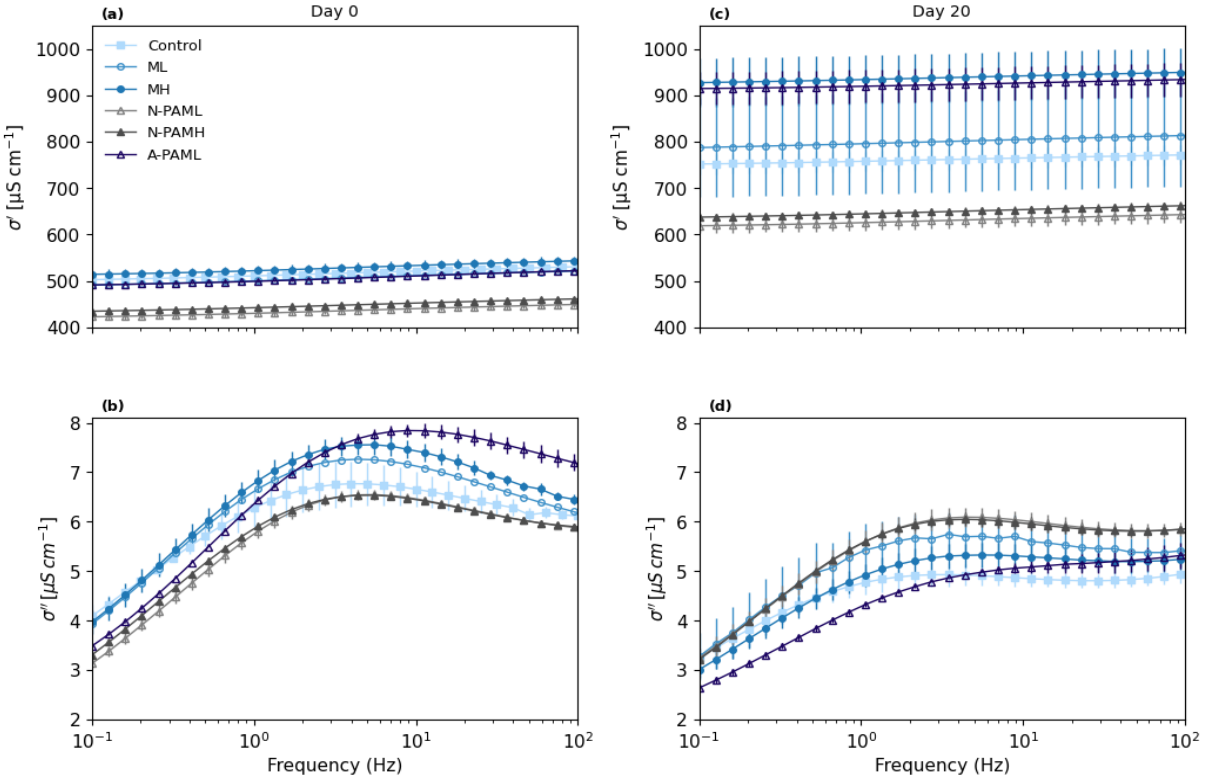

Figure 6. Frequency-dependent in-phase (σ′, a, c) and quadrature (σ″, b, d) conductivity of loess soil at day 0 (a, b) and day 20 (c, d) for all treatments: control, mucilage low (ML), mucilage high (MH), non-ionic PAM low (N-PAML), non-ionic PAM high (N-PAMH), and anionic PAM low (A-PAM)

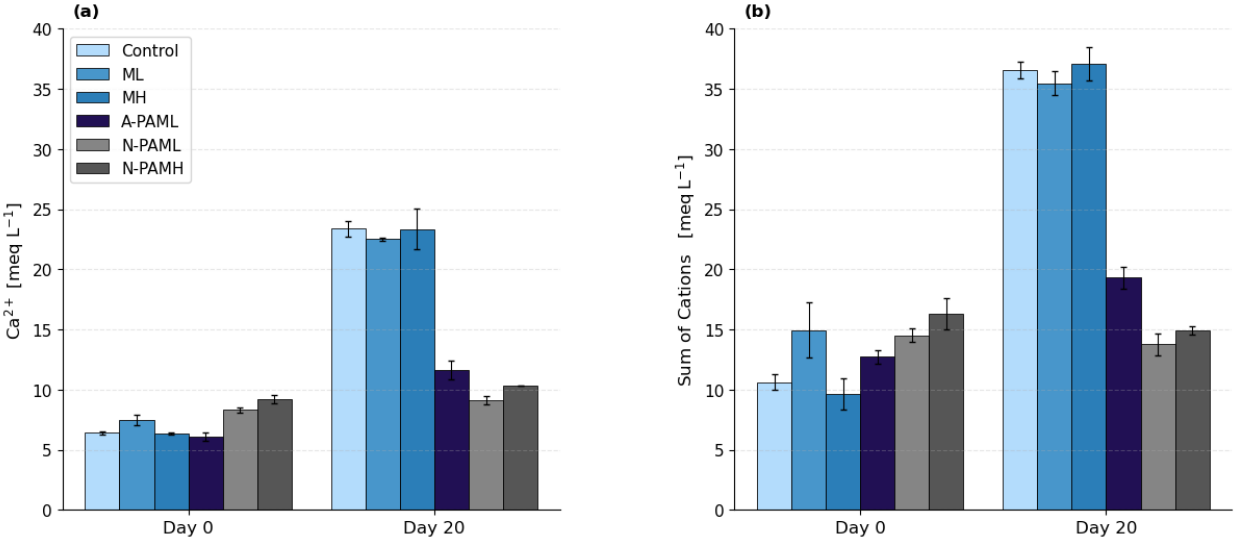

Figure 7. Soil solution chemistry of polymer-treated soils at day 0 and after 20 days of incubation. Shown are (a) Ca^{2+} concentration and (b) sum of cations in the effluents of control, mucilage (ML, MH), anionic PAM (A-PAML), and non-ionic PAM (N-PAML, N-PAMH)

277

https://doi.org/10.5194/egusphere-2026-3473
Preprint. Discussion started: 21 July 2026

4. Discussion

4.1 Effect of Polymer Stabilizers on Aggregate Stability: The Role of Microbial Activity

The treatment of soils with mucilage and A-PAM generated two distinct stabilization pathways. Mucilage treatment was dose responsive, resulting in an immediate increase in aggregate stability with MH generating higher stability than ML (Fig. 3). The soil stabilizing effect of mucilage has been reported previously (Morel et al., 1991; Traoré et al., 2000; Marsico et al., 2018). Soils treated with A-PAM were also dose-responsive and yielded more durable stabilization than the mucilage treatment. Even with a modest decline by day 20, stability remained significantly higher than under mucilage treatment (Fig. 3).

In parallel, mucilage addition (most pronounced for high concentration MH) stimulated high CO_2 emissions, in comparison to the addition of A-PAM (Fig. 2). This enhanced microbial response indicates that mucilage is a readily available carbon source, rich in labile polysaccharides (Nazari, 2021; Nazari et al., 2022; Even and Francesca Cotrufo, 2024). Hence, the high biodegradability of mucilage explains the decrease in soil stability by day 20. However, A-PAM is known to degrade slowly, often persisting in soils for years and providing little to no labile carbon to support microbial metabolism (Entry et al., 2008; Li et al., 2024). Beyond the lack of degradable carbon, the polymer's capacity to bind particles into larger, more stable aggregates can alter pore architecture, reduce oxygen diffusion, and limit the microscale exchange of water and nutrients (Caesar-TonThat et al., 2008; Mamedov et al., 2010, 2020). These changes can restrict microbial access to both carbon substrates and electron acceptors, further constraining respiration. It is important to note that CO_2 emission may also be attributed to calcite dissolution; therefore, differences among treatments are interpreted relative to the control, which may include both sources (Gallagher and Breecker, 2020; Sun et al., 2023).

Overall, these results show that mucilage induces a short-term increase in aggregation, which is subsequently reversed, due to its rapid biodegradation, whereas A-PAM elicits moderate microbial activity and therefore, provides a more persistent structural stabilization. In essence, mucilage triggers a transient, biologically driven response, while A-PAM delivers a longer-lasting, physicochemical reinforcement of soil structure.

4.2 Soil Structural Changes Affect Flow Pathways

The hydraulic behaviour of the treated soils followed two divergent evolutionary paths, mirroring the contrasting stability mechanisms of the polymers. Initially, the ML treatment induced higher flow heterogeneity, as evidenced by a higher dispersivity ($\alpha = 1.47\ cm$) compared to the control group ($\alpha = 0.55\ cm$) (Fig. 4a). These alterations in the flow path are likely attributable to modifications in the pore architecture, consistent with the observed increase in aggregate stability (section 4.1).

However, the convergence of the ML breakthrough curve to control-like behavior by day 20 demonstrates that these structural modifications were transient. This hydraulic reversion to baseline conditions aligns with the respiration data (Fig. 2), suggesting that as the mucilage is consumed, the associated structural modifications progressively reverse toward baseline

https://doi.org/10.5194/egusphere-2026-3473
Preprint. Discussion started: 21 July 2026

conditions (Dong et al., 2022; Xuan et al., 2022; Matisic et al., 2024). These findings contrast with previous studies reporting persistent structural improvements even following mucilage decomposition, often attributed to stable organo-mineral bonding or microbial byproducts (Morel et al., 1991; Traoré et al., 2000; Marsico et al., 2018). This discrepancy is likely attributable to differences in polymer concentration. While studies reporting long-term persistence typically applied mucilage at high rates (1-2% w/w), our study employed a considerably lower dosage (0.035-0.175% w/w). We hypothesize a concentration-dependent threshold effect: below a critical concentration, biodegradation outpaces the formation of secondary stabilizing mechanisms. This is supported by our aggregate stability data (Fig. 3), where the higher concentration treatment (MH, 0.175% w/w) maintained some aggregate stability throughout the incubation, whereas ML lost it.

Conversely, the A-PAML treatment exhibited persistent and intensifying transport heterogeneity. By day 20, the breakthrough curve displayed a pronounced tailing effect coinciding with the maintenance of high aggregate stability (Fig. 4b). This combination challenges the applicability of the standard ADE. Classical dispersion theory predicts that increased dispersivity should produce more spread-out but still symmetrical breakthrough curves. However, the A-PAML data present a systematic deviation from this prediction, with the model consistently overpredicting the initial rise (PV 0.5-0.8) and underpredicting the mid-section and tail (PV >1.2), failing to capture the characteristic S-shaped profile. This specific pattern of model failure is a hallmark of physical non-equilibrium, consistent with dual-domain transport, where A-PAM-induced structural reorganization promotes the formation of preferential flow pathways alongside hydraulically less accessible zones. This effectively partitions the pore network into mobile and immobile regions with limited mass exchange, rendering a single dispersion coefficient insufficient to describe solute transport (Van Genuchten and Wierenga, 1976; Corapcioglu and Wang, 1999; Bijeljic et al., 2011; Haggerty and Gorelick, 1995; de Vries et al., 2017).

4.3 SIP Signatures Reflect Changes in Soil Induced by Polymer Stabilizers

4.3.1 In-phase Conductivity (σ'): Electrolytic and Structural Controls

The temporal evolution of σ' reflect changes in pore-water chemistry, pore network geometry, and surface properties, as it is defined by the contributions of electrolyte bulk conductivity (σ'_w) and surface conductivity (σ'_s):

$$\sigma' = \frac{1}{F}\sigma'_w + \sigma'_s \quad (4)$$

where F is the formation factor, a geometric parameter describing the tortuosity of current pathways through the pore network:

$$F = \phi^{-m} \quad (5)$$

with ϕ as porosity and m as the cementation exponent. A consistent increasing trend in σ' was observed across all treatments from day 0 to day 20 (Fig. 5a). However, the magnitude of this increase and its relationship with effluent chemistry varied substantially among treatments, indicating that distinct mechanisms governed the evolution of σ' in each case.

https://doi.org/10.5194/egusphere-2026-3473
Preprint. Discussion started: 21 July 2026

In the control and ML treatments, σ' increased by 50% to 60% by day 20, corresponding to a 200-266% rise in effluent Ca^{2+} concentration (Fig. 7a, b). This concurrent rise suggests that Ca^{2+}, released through continuous dissolution of carbonate minerals (mainly calcite) abundant in loess soils, was the dominant driver of pore water conductivity (σ'_w). which in turn governed the rise in σ' observed in these treatments.

The MH treatment, however, appeared to decouple this relationship. Despite reaching a nearly identical terminal cation concentration (~36 meq L^{-1}) in the effluent (Fig. 7b), the MH treatment exhibited an 80% increase in σ',substantially greater than the 50%-60% observed in control and ML treatments (Fig. 5a). Since σ'_s is jointly reflected in both $\sigma'$and σ'', and since no differential increase in σ'' was observed in the MH treatment relative to control or ML (Fig. 5b), surface conductance is unlikely to account for this discrepancy. We therefore suggest that the elevated σ' in MH, may reflect a structural change in pore geometry, specifically a reduction in F. The enhanced aggregate stability observed in the MH treatment (Fig. 3) provides the structural basis for this interpretation: stable aggregates resist slaking and pore collapse upon wetting, preserving the interaggregate contact network that constitutes the primary conducting pathway in aggregated soils (Bronick and Lal, 2005; Menon et al., 2020; Zhang et al., 2023). Better aggregated soils tend to sustain greater pore network connectivity upon saturation, not necessarily through improved individual flow paths but through a larger number of connected pathways remaining open, effectively reducing the tortuosity of current-conducting pathways and thereby lowering F (Archie, 1942; Bernabé et al., 2011; Geers-Lucas et al., 2025).

The A-PAML treatment exhibited a distinctly different pattern: σ' increased comparably to MH by day 20 (Fig. 5a), yet paradoxically yielded the lowest effluent Ca^{2+} concentrations (Fig. 7a). Unlike the control and ML treatments where σ' increase tracked pore water ionic strength, and unlike MH where structural improvements in connectivity were proposed, neither mechanism straightforwardly accounts for the A-PAML pattern. We hypothesize that this disparity arises from the intense stabilization induced by the anionic polymer, which promotes the formation of stable micro-aggregates and enhances structural heterogeneity characteristic of a dual-porosity system. This structure is likely characterized by significant volumes of immobile water within the intra-aggregate pores. While dissolved ions accumulate within these zones and remain part of the continuous conductive phase sensed by SIP, they are hydraulically isolated from the active flow paths and thus do not appear in the leachate (Cote et al., 2000; Rhoades et al., 1976). Consequently, the A-PAML treatment effectively creates a conductive reservoir that is physically trapped within the soil structure, elevating σ'independently of the leachate chemistry.

The N-PAM treatments were included as a reference to isolate the effect of neutral polymer adsorption on the electrical interface, independent of significant structural aggregation. Consistent with this role, both N-PAML and N-PAMH exhibited consistently lower absolute σ' values from day 0 throughout the experiment, despite similar initial cation concentrations across all treatments (Fig. 5a). Since σ'_w was approximately equal across treatments at day 0, the initial suppression of σ' implicates either an increase in F or a reduction in σ'_s as the primary cause (Eq. 4). As nonionic PAM adsorbs onto soil surfaces primarily through weaker Van der Waals forces or hydrogen bonds, rather than the electrostatic interactions characteristic of charged

https://doi.org/10.5194/egusphere-2026-3473
Preprint. Discussion started: 21 July 2026

polymers, its capacity to induce structural reorganization of the pore network is comparatively limited (Theng, 1982; McGuire et al., 2006; Abu-Zreig, 2006), making a substantial increase in F an unlikely explanation and pointing instead to a reduction in σ_s' as the dominant mechanism. This interpretation is supported by observations of neutralized zeta potential upon nonionic polymer adsorption onto mineral surfaces (Choo et al., 2020), consistent with a surface coating that reduces the expression of surface charge available for counter-ion accumulation. Additional support comes from the effluent chemistry: while cation concentrations in control, ML and MH treatments rose substantially by day 20, N-PAM effluent concentrations remained largely unchanged (Fig. 7b). This is consistent with evidence that nonionic PAM can inhibit calcite dissolution through hydrogen bonding and surface complexation (Ji et al., 2021). Together, these observations suggest that nonionic PAM adsorption simultaneously suppressed σ_s' through surface charge screening and limited the development of σ_w' by inhibiting mineral dissolution, both arising from the same interfacial coating established upon polymer application. The near-identical responses of N-PAML and N-PAMH further suggest that surface saturation was achieved even at the lower polymer concentration, consistent with the tendency of PAM adsorption on mineral surfaces to reach a plateau as available surface sites become occupied (Graveling et al., 1997).

4.3.2 Quadrature Conductivity (σ''): Interfacial Polarization and Surface Effects

While σ' conductivity reflects bulk solution and pore network properties, σ'' provides a direct probe of the soil-water interface and the polarization of the EDL (Vinegar and Waxman, 1984; Binley and Slater, 2020). At day 0, σ'' was highest in the A-PAML and mucilage treatments, reaching comparable values of 7.3-7.8 µS cm^{-1}, while the control and both N-PAM treatments displayed lower values of approximately 6.5-6.7 µS cm^{-1} (Fig. 5b). This initial differentiation reflects the charged nature of the applied polymers: both carry negative surface charge (Deng et al., 2006; Dobrynin and Rubinstein, 2005; Garcia e Silva et al., 2022; Solanki et al., 2024), and their adsorption onto mineral surfaces increases the density of active interfacial sites available for polarization, thereby enhancing σ'' relative to the control (Revil, 2012; Revil and Skold, 2011). In contrast, the adsorption of neutral N-PAM does not enrich the EDL, and its σ'' values at day 0 were similar to the control, consistent with the absence of charge-dependent interfacial interactions upon polymer application.

Following the initial state, σ'' declined progressively over the 20-day incubation in all treatments except N-PAM (Fig. 5b). We attribute this general decline primarily to calcite dissolution, which continuously removes reactive mineral surfaces available for EDL polarization. As calcite dissolves, the abundance of active interfacial sites diminishes, reducing the polarization response sensed by σ'' over time. This mechanism is consistent with previous observations in calcareous soils (Altzitser et al., 2025) and is expected to operate across all treatments where mineral dissolution is not inhibited.

In the mucilage treatments, biodegradation of the organic coating provided an additional pathway for σ'' decline, operating alongside calcite dissolution. The progressive loss of mucilage is supported by the elevated CO_2 respiration rates (Fig. 2), the concurrent decline in aggregate stability over time (Fig. 3), and the convergence of breakthrough curves toward control

https://doi.org/10.5194/egusphere-2026-3473
Preprint. Discussion started: 21 July 2026

behaviour by day 20 (Fig. 4b). As the mucilage coating was progressively consumed, its contribution to polarizable interfacial sites diminished accordingly. Notably, both ML and MH converged toward similar final σ'' values by day 20 regardless of their initial concentration differences, suggesting that mucilage no longer contributed meaningfully to soil polarization once biodegradation was complete.

The A-PAML treatment presents a more complex picture. Despite showing the steepest total decline in σ'' of approximately 35% from its initial value (Fig. 5b), A-PAML exhibited no evidence of elevated microbial respiration (Fig. 2), ruling out biodegradation as an explanation. We suggest that the structural reorganization induced by A-PAM provides an alternative mechanism. As established in section 4.3.1, A-PAM promotes the formation of stable micro-aggregates and the development of a dual-porosity system characterized by mobile and immobile water domains. Within the immobile intra-aggregate pores, ions progressively accumulate but become physically restricted from oscillating in response to the alternating electric field. This restriction reduces the effective polarizable interface sensed by σ'', producing a decline comparable in magnitude to that driven by biodegradation in the mucilage treatments, yet through an entirely different pathway. This interpretation is consistent with the pronounced tailing and dual-domain transport behavior demonstrated by the breakthrough experiments (Fig. 4b).

In contrast, σ'' in both N-PAM treatments remained nearly constant throughout the entire 20-day incubation (Fig. 5b), exhibiting only minor decreases of approximately 7%. This temporal stability sets N-PAM apart from all other treatments and reinforces the surface screening interpretation developed in section 4.3.1. The neutral polymer coating effectively decoupled the mineral interface from the evolving bulk solution chemistry, inhibiting calcite dissolution and thereby preserving the reactive mineral surfaces that drove σ'' decline in all other treatments. This temporal stability of σ'' thus serves as geoelectrical confirmation of the surface screening role of N-PAM, and further validates its use in this study as a reference treatment for isolating charge-independent polymer adsorption effects.

The spectral distribution of σ'' provides additional structural insights that complement the temporal trends discussed above (Fig. 6b, 6d). At day 0, while most treatments displayed peak frequencies in the range of 4 Hz to 5.5 Hz, the A-PAML peak was notably shifted to a higher value of approximately 8.9 Hz. In SIP theory, the relaxation frequency is inversely proportional to the square of the characteristic polarization length scale ($f_{peak} \propto D/L^2$, where L represents the characteristic pore or grain size), such that higher peak frequencies correspond to shorter characteristic length scales (Slater et al., 2007; Bücker and Hördt, 2013; Binley and Slater, 2020; Schwartz et al., 2020). We suggest that this shift reflects the reorganization of fine soil particles into microaggregates induced by A-PAM, creating a pore network dominated by smaller intra-aggregate pores compared to the larger interaggregate pores of unamended soil. This interpretation is consistent with the aggregate stability results showing that A-PAML produced the most stable aggregates of all treatments (Fig. 3) and with the dual-porosity behaviour indicated by the breakthrough experiments (Fig. 4).

By day 20, the A-PAML σ'' spectrum exhibited pronounced flattening and broadening (Fig. 6d). While all treatments showed some degree of spectral flattening relative to day 0, the change was most dramatic in A-PAML. This broadening indicates that

https://doi.org/10.5194/egusphere-2026-3473
Preprint. Discussion started: 21 July 2026

the initially relatively uniform pore size distribution became increasingly heterogeneous over time, producing a wide distribution of relaxation length scales, consistent with the progressive development of the dual porosity system proposed above. The near-stability of the N-PAM spectrum further supports the surface screening interpretation: by limiting the geochemical interactions that drove structural evolution in other treatments, the neutral polymer coating effectively preserved the original pore size distribution throughout the incubation period.

5. Conclusions

This study characterized the diverse stabilization pathways induced by natural (mucilage) and synthetic (A-PAM) polymers. By coupling traditional soil characterization with continuous SIP monitoring, the study tracked the temporal evolution of aggregate stability, hydraulic connectivity, and microbial activity over a 20-day incubation period.

The application of SIP facilitated the detection of micro-scale structural dynamics that remained largely obscured by standard ex situ and effluent analyses. Specifically, SIP signatures identified the formation of a 'conductive reservoir' within the A-PAM-treated soil, where dissolved ions remained part of the conductive phase despite being hydraulically isolated from active flow paths. Furthermore, high-frequency shifts in the quadrature conductivity (σ'') served as an indicator of shorter characteristic polarization length scales. These measurements provided geoelectrical evidence for the development of a persistent, hierarchical pore system and a dual-porosity regime that traditional protocols could only retrospectively confirm. Methodologically, the study utilized N-PAM as a reference to isolate surface screening effects and distinguish them from active interfacial polarization, while demonstrating SIP's sensitivity to the contrasting charge densities and conformations of the polymers.

The findings reveal a clear performance gap based on polymer persistence and concentration thresholds. A concentration of 0.035% (w/w) was applied to represent typical environmental concentrations found in the natural rhizosphere. At this baseline, mucilage proved insufficient to maintain sustained stabilization; rapid microbial consumption of the polymer led to progressive loss of aggregate stability and reversion toward baseline hydraulic behaviour. The enhanced 0.175% (w/w) dosage demonstrated a dose-responsive increase in initial stability and maintained a higher degree of aggregate stability throughout the incubation, yet followed the same degradation trajectory as ML, confirming that the stabilization benefits of mucilage remain fundamentally governed by its degradation kinetics regardless of initial concentration. Ultimately, A-PAM delivered a longer-lasting, physicochemical reinforcement of the soil matrix, whereas the structural benefits of mucilage remained strictly governed by degradation kinetics.

While A-PAM provides superior mechanical persistence, its application entails broader environmental implications, including the hydraulic isolation of intra-aggregate domains and the subsequent risk of pollutant entrapment within the soil matrix. As a synthetic additive, A-PAM remains an external ecosystem input. Conversely, although CSM was also introduced as an external stabilizer in this investigation, it serves as a natural, root-derived analogue that actively stimulates the soil microbiome.

https://doi.org/10.5194/egusphere-2026-3473
Preprint. Discussion started: 21 July 2026

Despite the transient structural benefits observed at current dosages, the external application of CSM offers a potential pathway toward self-sustaining stabilization cycles. It is hypothesized that under optimized conditions or specific concentration thresholds, the microbial degradation of mucilage may facilitate the production of bacterial Extracellular Polymeric Substances (EPS). This process could theoretically transition the soil from temporary physical binding to persistent biogenic cementation, creating a virtuous cycle of structural reinforcement. Exploring these biologically-mediated stabilization pathways, alongside the long-term transport dynamics in dual-porosity systems, remains a critical frontier for sustainable soil management.

Code and data availability

Data will be made available upon request.

Author contributions

S.A. Altzitser: Writing – original draft, Writing – review & editing, Conceptualization, Methodology, Investigation, Formal analysis, Data curation, Visualization, Project administration. **Y.G Mishael:** Supervision, Writing – review & editing, Resources, Conceptualization. **N. Schwartz:** Supervision, Writing – review & editing, Methodology, Resources, Conceptualization.

Competing interests

The contact author has declared that none of the authors has any competing interests.

Disclaimer

Copernicus Publications remains neutral with regard to jurisdictional claims in published maps and institutional affiliations.

Acknowledgements

All authors contributed to the conceptualization, discussion, and writing of the manuscript.

Financial support

This research did not receive any specific grant from funding agencies in the public, commercial, or not-for-profit sectors.

References

Abu-Zreig, M.: Control of Rainfall-Induced Soil Erosion with Various Types of Polyacrylamide (8 pp), J. Soils Sediments, 6, 137–144, https://doi.org/10.1065/jss2006.04.152, 2006.

https://doi.org/10.5194/egusphere-2026-3473
Preprint. Discussion started: 21 July 2026

Albalasmeh, A. A., Hamdan, E. H., Gharaibeh, M. A., and Hanandeh, A. E.: Improving aggregate stability and hydraulic properties of Sandy loam soil by applying polyacrylamide polymer, Soil Tillage Res., 206, 104821, https://doi.org/10.1016/j.still.2020.104821, 2021.

Alletto, L., Coquet, Y., Benoit, P., Heddadj, D., and Barriuso, E.: Tillage management effects on pesticide fate in soils. A review, Agron. Sustain. Dev., 30, 367–400, https://doi.org/10.1051/agro/2009018, 2010.

Almajed, A., Lemboye, K., and Moghal, A. A. B.: A Critical Review on the Feasibility of Synthetic Polymers Inclusion in Enhancing the Geotechnical Behavior of Soils, Polymers, 14, 5004, https://doi.org/10.3390/polym14225004, 2022.

Altzitser, S. S., Mishael, Y. G., and Schwartz, N.: Organic pollutant oxidation on manganese oxides in soils – the role of calcite indicated by geoelectrical and chemical analyses, SOIL, 11, 95–104, https://doi.org/10.5194/soil-11-95-2025, 2025.

Archie, G. E.: The Electrical Resistivity Log as an Aid in Determining Some Reservoir Characteristics, Trans. AIME, 146, 54–62, https://doi.org/10.2118/942054-G, 1942.

Ayral-Cinar, D. and Demond, A. H.: Diffusion of Iodide in Low Permeability Clayey Soils, ATHENS J. Sci., 4, 187–198, https://doi.org/10.30958/ajs.4-3-1, 2017.

Ball, B. C.: Soil structure and greenhouse gas emissions: a synthesis of 20 years of experimentation, Eur. J. Soil Sci., 64, 357–373, https://doi.org/10.1111/ejss.12013, 2013.

Bartha, R. and Pramer, D.: Features of a Flask and Method for Measuring the Persistence and Biological Effects of Pesticides in Soil, Soil Sci., 100, 68, 1965.

Bernabé, Y., Zamora, M., Li, M., Maineult, A., and Tang, Y. B.: Pore connectivity, permeability, and electrical formation factor: A new model and comparison to experimental data: CONNECTIVITY, PERMEABILITY, J. Geophys. Res. Solid Earth, 116, n/a-n/a, https://doi.org/10.1029/2011JB008543, 2011.

Bijeljic, B., Rubin, S., Scher, H., and Berkowitz, B.: Non-Fickian transport in porous media with bimodal structural heterogeneity, J. Contam. Hydrol., 120–121, 213–221, https://doi.org/10.1016/j.jconhyd.2010.05.007, 2011.

Binley, A. and Kemna, A.: DC Resistivity and Induced Polarization Methods, Hydrogeophysics, 129–156, https://doi.org/10.1007/1-4020-3102-5_5, 2005.

Binley, A. and Slater, L.: Resistivity and Induced Polarization: Theory and Applications to the Near-Surface Earth, Resist. Induc. Polariz., https://doi.org/10.1017/9781108685955, 2020.

Borrelli, P., Alewell, C., Alvarez, P., Anache, J. A. A., Baartman, J., Ballabio, C., Bezak, N., Biddoccu, M., Cerdà, A., Chalise, D., Chen, S., Chen, W., De Girolamo, A. M., Gessesse, G. D., Deumlich, D., Diodato, N., Efthimiou, N., Erpul, G., Fiener, P., Freppaz, M., Gentile, F., Gericke, A., Haregeweyn, N., Hu, B., Jeanneau, A., Kaffas, K., Kiani-Harchegani, M., Villuendas, I. L., Li, C., Lombardo, L., López-Vicente, M., Lucas-Borja, M. E., Märker, M., Matthews, F., Miao, C., Mikoš, M., Modugno, S., Möller, M., Naipal, V., Nearing, M., Owusu, S., Panday, D., Patault, E., Patriche, C. V., Poggio, L., Portes, R., Quijano, L., Rahdari, M. R., Renima, M., Ricci, G. F., Rodrigo-Comino, J., Saia, S., Samani, A. N., Schillaci, C., Syrris, V., Kim, H. S., Spinola, D. N., Oliveira, P. T., Teng, H., Thapa, R., Vantas, K., Vieira, D., Yang, J. E., Yin, S., Zema, D. A., Zhao, G., and Panagos, P.: Soil erosion modelling: A global review and statistical analysis, Sci. Total Environ., 780, 146494, https://doi.org/10.1016/j.scitotenv.2021.146494, 2021.

Bozyigit, I., Zingil, H. O., and Altun, S.: Performance of eco-friendly polymers for soil stabilization and their resistance to freeze–thaw action, Constr. Build. Mater., 379, 131133, https://doi.org/10.1016/j.conbuildmat.2023.131133, 2023.

https://doi.org/10.5194/egusphere-2026-3473
Preprint. Discussion started: 21 July 2026

Brax, M., Buchmann, C., Kenngott, K., Schaumann, G. E., and Diehl, D.: Influence of the physico-chemical properties of root mucilage and model substances on the microstructural stability of sand, Biogeochemistry, 147, 35–52, https://doi.org/10.1007/s10533-019-00626-w, 2020.

Bronick, C. J. and Lal, R.: Soil structure and management: a review, Geoderma, 124, 3–22, https://doi.org/10.1016/j.geoderma.2004.03.005, 2005.

Brusseau, M. L., Gerstl, Z., Augustijn, D., and Rao, P. S. C.: Simulating solute transport in an aggregated soil with the dual-porosity model: measured and optimized parameter values, J. Hydrol., 163, 187–193, https://doi.org/10.1016/0022-1694(94)90028-0, 1994.

Caesar-TonThat, T. C., Busscher, W. J., Novak, J. M., Gaskin, J. F., and Kim, Y.: Effects of polyacrylamide and organic matter on microbes associated to soil aggregation of Norfolk loamy sand, Appl. Soil Ecol., 40, 240–249, https://doi.org/10.1016/j.apsoil.2008.04.008, 2008.

Capitani, M. I., Ixtaina, V. Y., Nolasco, S. M., and Tomás, M. C.: Microstructure, chemical composition and mucilage exudation of chia (Salvia hispanica L.) nutlets from Argentina, J. Sci. Food Agric., 93, 3856–3862, https://doi.org/10.1002/jsfa.6327, 2013.

Carminati, A. and Vetterlein, D.: Plasticity of rhizosphere hydraulic properties as a key for efficient utilization of scarce resources, Ann. Bot., 112, 277–290, https://doi.org/10.1093/aob/mcs262, 2013.

Choo, H., Choi, Y., Kim, Y.-U., Lee, W., and Lee, C.: Compressibility and hydraulic conductivity of calcium bentonite treated with pH-responsive polymer, Geomech. Eng., 22, 329–337, https://doi.org/10.12989/gae.2020.22.4.329, 2020.

Corapcioglu, M. Y. and Wang, S.: Dual-porosity groundwater contaminant transport in the presence of colloids, Water Resour. Res., 35, 3261–3273, https://doi.org/10.1029/1999WR900122, 1999.

Cote, C. M., Bristow, K. L., and Ross, P. J.: Increasing the efficiency of solute leaching: impacts of flow interruption with drainage of the “preferential flow paths,” J. Contam. Hydrol., 43, 191–209, https://doi.org/10.1016/S0169-7722(00)00087-5, 2000.

Deng, Y., Dixon, J. B., and White, G. N.: Adsorption of Polyacrylamide on Smectite, Illite, and Kaolinite, Soil Sci. Soc. Am. J., 70, 297–304, https://doi.org/10.2136/sssaj2005.0200, 2006.

Dobrynin, A. V. and Rubinstein, M.: Theory of polyelectrolytes in solutions and at surfaces, Prog. Polym. Sci., 30, 1049–1118, https://doi.org/10.1016/j.progpolymsci.2005.07.006, 2005.

Dong, L., Zhang, W., Xiong, Y., Zou, J., Huang, Q., Xu, X., Ren, P., and Huang, G.: Impact of short-term organic amendments incorporation on soil structure and hydrology in semiarid agricultural lands, Int. Soil Water Conserv. Res., 10, 457–469, https://doi.org/10.1016/j.iswcr.2021.10.003, 2022.

Dor, M., Emmanuel, S., Brumfeld, V., Levy, G. J., and Mishael, Y. G.: Microstructural changes in soils induced by wetting and drying: Effects on atrazine mobility, Land Degrad. Dev., 30, 746–755, https://doi.org/10.1002/ldr.3256, 2019.

Entry, J. A., Sojka, R. E., and Hicks, B. J.: Carbon and nitrogen stable isotope ratios can estimate anionic polyacrylamide degradation in soil, Geoderma, 145, 8–16, https://doi.org/10.1016/j.geoderma.2007.12.015, 2008.

Even, R. J. and Francesca Cotrufo, M.: The ability of soils to aggregate, more than the state of aggregation, promotes protected soil organic matter formation, Geoderma, 442, 116760, https://doi.org/10.1016/j.geoderma.2023.116760, 2024.

https://doi.org/10.5194/egusphere-2026-3473
Preprint. Discussion started: 21 July 2026

559 Gallagher, T. M. and Breecker, D. O.: The Obscuring Effects of Calcite Dissolution and Formation on Quantifying Soil
560 Respiration, Glob. Biogeochem. Cycles, 34, e2020GB006584, https://doi.org/10.1029/2020GB006584, 2020.

561 Garcia e Silva, L. L., Alves Bastos, R., Souza Lima, G. V., de Souza Soares, L., Selia dos Reis Coimbra, J., Arêdes Martins,
562 M., and de Castro Santana, R.: Stabilizing Properties of Chia Seed Mucilage on Dispersions and Emulsions at Different pHs,
563 Food Biophys., 17, 568–574, https://doi.org/10.1007/s11483-022-09742-x, 2022.

564 Garland, G., Koestel, J., Johannes, A., Heller, O., Doetterl, S., Or, D., and Keller, T.: Perspectives on the misconception of
565 levitating soil aggregates, SOIL, 10, 23–31, https://doi.org/10.5194/soil-10-23-2024, 2024.

566 Geers-Lucas, M., Leue, M., Schlüter, S., and Sommer, M.: Long-term improvement of subsoil pore structure in sandy soils by
567 meliorative fractional deep tillage, Geoderma, 463, 117556, https://doi.org/10.1016/j.geoderma.2025.117556, 2025.

568 Gerke, H. H. and van Genuchten, M. T.: A dual-porosity model for simulating the preferential movement of water and solutes
569 in structured porous media, Water Resour. Res., 29, 305–319, https://doi.org/10.1029/92WR02339, 1993.

570 Graveling, G. J., Vala Ragnarsdottir, K., Allen, G. C., Eastman, J., Brady, P. V., Balsley, S. D., and Skuse, D. R.: Controls on
571 polyacrylamide adsorption to quartz, kaolinite, and feldspar, Geochim. Cosmochim. Acta, 61, 3515–3523,
572 https://doi.org/10.1016/S0016-7037(97)00175-0, 1997.

573 Huang, J., Kogbara, R. B., Hariharan, N., Masad, E. A., and Little, D. N.: A state-of-the-art review of polymers used in soil
574 stabilization, Constr. Build. Mater., 305, 124685, https://doi.org/10.1016/j.conbuildmat.2021.124685, 2021.

575 Ji, Y., Walkinshaw, C., Belshaw, G., and Vandeginste, V.: Effect of polyacrylamide friction reducer on calcite dissolution rate
576 at 25 °C and implication for hydraulic fracturing, J. Nat. Gas Sci. Eng., 87, 103770,
577 https://doi.org/10.1016/j.jngse.2020.103770, 2021.

578 Kemper, W. D. and Rosenau, R. C.: Aggregate Stability and Size Distribution, in: Methods of Soil Analysis, John Wiley &
579 Sons, Ltd, 425–442, https://doi.org/10.2136/sssabookser5.1.2ed.c17, 1986.

580 Kessouri, P., Furman, A., Huisman, J. A., Martin, T., Mellage, A., Ntarlagiannis, D., Bücker, M., Ehosioke, S., Fernandez, P.,
581 Flores-Orozco, A., Kemna, A., Nguyen, F., Pilawski, T., Saneiyan, S., Schmutz, M., Schwartz, N., Weigand, M., Wu, Y.,
582 Zhang, C., and Placencia-Gomez, E.: Induced polarization applied to biogeophysics: recent advances and future prospects,
583 Surf. Geophys., 17, 595–621, https://doi.org/10.1002/nsg.12072, 2019.

584 Kroener, E., Zarebanadkouki, M., Kaestner, A., and Carminati, A.: Nonequilibrium water dynamics in the rhizosphere: How
585 mucilage affects water flow in soils, Water Resour. Res., 50, 6479–6495, https://doi.org/10.1002/2013WR014756, 2014.

586 Lal, R.: Soil degradation by erosion, Land Degrad. Dev., 12, 519–539, https://doi.org/10.1002/ldr.472, 2001.

587 Le Bissonnais, Y.: Aggregate stability and assessment of soil crustability and erodibility: I. Theory and methodology, Eur. J.
588 Soil Sci., 47, 425–437, https://doi.org/10.1111/j.1365-2389.1996.tb01843.x, 1996.

589 Lee, S. S., Chang, S. X., Chang, Y.-Y., and Ok, Y. S.: Commercial versus synthesized polymers for soil erosion control and
590 growth of Chinese cabbage, SpringerPlus, 2, 534, https://doi.org/10.1186/2193-1801-2-534, 2013.

591 Leroy, B. L. M., Herath, H. M. S. K., Sleutel, S., De Neve, S., Gabriels, D., Reheul, D., and Moens, M.: The quality of
592 exogenous organic matter: short-term effects on soil physical properties and soil organic matter fractions, Soil Use Manag.,
593 24, 139–147, https://doi.org/10.1111/j.1475-2743.2008.00142.x, 2008.

https://doi.org/10.5194/egusphere-2026-3473
Preprint. Discussion started: 21 July 2026

Li, J., Usman, M., Arslan, M., and Gamal El-Din, M.: Molecular and microbial insights towards anaerobic biodegradation of anionic polyacrylamide in oil sands tailings, Water Res., 258, 121757, https://doi.org/10.1016/j.watres.2024.121757, 2024.

Mamedov, A. I., Wagner, L. E., Huang, C., Norton, L. D., and Levy, G. J.: Polyacrylamide Effects on Aggregate and Structure Stability of Soils with Different Clay Mineralogy, Soil Sci. Soc. Am. J., 74, 1720–1732, https://doi.org/10.2136/sssaj2009.0279, 2010.

Mamedov, A. I., Tsunekawa, A., Tsubo, M., Fujimaki, H., Ekberli, I., Şeker, C., Öztürk, H. S., Cerdà, A., and Levy, G. J.: Structure Stability of Cultivated Soils from Semi-Arid Region: Comparing the Effects of Land Use and Anionic Polyacrylamide Application, Agronomy, 10, 2010, https://doi.org/10.3390/agronomy10122010, 2020.

Marsico, A. D., Scrano, L., Labella, R., Lanzotti, V., Rossi, R., Cox, L., Perniola, M., and Amato, M.: Mucilage from fruits/seeds of chia (Salvia hispanica L.) improves soil aggregate stability, Plant Soil, 425, 57–69, https://doi.org/10.1007/S11104-018-3565-1/FIGURES/6, 2018.

Matisic, M., Dugan, I., and Bogunovic, I.: Challenges in Sustainable Agriculture—The Role of Organic Amendments, Agriculture, 14, 643, https://doi.org/10.3390/agriculture14040643, 2024.

McGuire, M. J., Addai-Mensah, J., and Bremmell, K. E.: Spectroscopic investigation of the adsorption mechanisms of polyacrylamide polymers onto iron oxide particles, J. Colloid Interface Sci., 299, 547–555, https://doi.org/10.1016/j.jcis.2006.03.015, 2006.

Mellage, A., Zakai, G., Efrati, B., Pagel, H., and Schwartz, N.: Paraquat sorption- and organic matter-induced modifications of soil spectral induced polarization (SIP) signals, Geophys. J. Int., 229, 1422–1433, https://doi.org/10.1093/GJI/GGAB531, 2022.

Menon, M., Mawodza, T., Rabbani, A., Blaud, A., Lair, G. J., Babaei, M., Kercheva, M., Rousseva, S., and Banwart, S.: Pore system characteristics of soil aggregates and their relevance to aggregate stability, Geoderma, 366, 114259, https://doi.org/10.1016/j.geoderma.2020.114259, 2020.

Morel, J. L., Habib, L., Plantureux, S., and Guckert, A.: Influence of maize root mucilage on soil aggregate stability, Plant Soil, 136, 111–119, https://doi.org/10.1007/BF02465226, 1991.

Nazari, M.: Plant mucilage components and their functions in the rhizosphere, Rhizosphere, 18, 100344, https://doi.org/10.1016/j.rhisph.2021.100344, 2021.

Nazari, M., Bickel, S., Benard, P., Mason-Jones, K., Carminati, A., and Dippold, M. A.: Biogels in Soils: Plant Mucilage as a Biofilm Matrix That Shapes the Rhizosphere Microbial Habitat, Front. Plant Sci., 12, https://doi.org/10.3389/fpls.2021.798992, 2022.

Pandey, S., Kumar, P., Zlatic, M., Nautiyal, R., and Panwar, V. P.: Recent advances in assessment of soil erosion vulnerability in a watershed, Int. Soil Water Conserv. Res., 9, 305–318, https://doi.org/10.1016/j.iswcr.2021.03.001, 2021.

Pimentel, D. and Kounang, N.: Ecology of Soil Erosion in Ecosystems, Ecosystems, 1, 416–426, https://doi.org/10.1007/s100219900035, 1998.

Pye, K.: Loess, Prog. Phys. Geogr. Earth Environ., 8, 176–217, https://doi.org/10.1177/030913338400800202, 1984.

Rabot, E., Wiesmeier, M., Schlüter, S., and Vogel, H.-J.: Soil structure as an indicator of soil functions: A review, Geoderma, 314, 122–137, https://doi.org/10.1016/j.geoderma.2017.11.009, 2018.

https://doi.org/10.5194/egusphere-2026-3473
Preprint. Discussion started: 21 July 2026

Revil, A.: Spectral induced polarization of shaly sands: Influence of the electrical double layer, Water Resour. Res., 48, https://doi.org/10.1029/2011WR011260, 2012.

Revil, A. and Skold, M.: Salinity dependence of spectral induced polarization in sands and sandstones, Geophys. J. Int., 187, 813–824, https://doi.org/10.1111/j.1365-246X.2011.05181.x, 2011.

Reynolds, J. M.: An Introduction to Appiled and Environmetal Geophysich, 712, 2011.

Rhoades, J. D., Raats, P. a. C., and Prather, R. J.: Effects of Liquid-phase Electrical Conductivity, Water Content, and Surface Conductivity on Bulk Soil Electrical Conductivity, Soil Sci. Soc. Am. J., 40, 651–655, https://doi.org/10.2136/sssaj1976.03615995004000050017x, 1976.

Rinot, O., Levy, G. J., Steinberger, Y., Svoray, T., and Eshel, G.: Soil health assessment: A critical review of current methodologies and a proposed new approach, Sci. Total Environ., 648, 1484–1491, https://doi.org/10.1016/j.scitotenv.2018.08.259, 2019.

Schwartz, N. and Furman, A.: Spectral induced polarization signature of soil contaminated by organic pollutant: Experiment and modeling, J. Geophys. Res. Solid Earth, 117, 10203, https://doi.org/10.1029/2012JB009543, 2012.

Schwartz, N., Huisman, J. A., and Furman, A.: The effect of NAPL on the electrical properties of unsaturated porous media, Geophys. J. Int., 188, 1007–1011, https://doi.org/10.1111/J.1365-246X.2011.05332.X/2/188-3-1007-FIG002.JPEG, 2012.

Seybold, C. A.: Polyacrylamide review: Soil conditioning and environmental fate, Commun. Soil Sci. Plant Anal., 25, 2171–2185, https://doi.org/10.1080/00103629409369180, 1994.

Shahane, A. A. and Shivay, Y. S.: Soil Health and Its Improvement Through Novel Agronomic and Innovative Approaches, Front. Agron., 3, https://doi.org/10.3389/fagro.2021.680456, 2021.

Solanki, D., Dhungana, P., Tan, Q. Y., Badin, R., Bhandari, B., Sahu, J. K., and Prakash, S.: Assessing the functional and physicochemical properties of chia seed mucilage extracted using an innovative extraction method, Food Hydrocoll., 156, 110342, https://doi.org/10.1016/j.foodhyd.2024.110342, 2024.

Soltani, A., Deng, A., Taheri, A., and O'Kelly, B. C.: Intermittent swelling and shrinkage of a highly expansive soil treated with polyacrylamide, J. Rock Mech. Geotech. Eng., 14, 252–261, https://doi.org/10.1016/j.jrmge.2021.04.009, 2022.

Sun, Z., Meng, F., and Zhu, B.: Influencing factors and partitioning methods of carbonate contribution to CO2 emissions from calcareous soils, Soil Ecol. Lett., 5, 6–20, https://doi.org/10.1007/s42832-022-0139-1, 2023.

Theng, B. K. G.: Clay-Polymer Interactions: Summary and Perspectives, Clays Clay Miner., 30, 1–10, https://doi.org/10.1346/CCMN.1982.0300101, 1982.

Traoré, O., Groleau-Renaud, V., Plantureux, S., Tubeileh, A., and Boeuf-Tremblay, V.: Effect of root mucilage and modelled root exudates on soil structure, Eur. J. Soil Sci., 51, 575–581, https://doi.org/10.1111/j.1365-2389.2000.00348.x, 2000.

Tully, K. L. and McAskill, C.: Promoting soil health in organically managed systems: a review, Org. Agric., 10, 339–358, https://doi.org/10.1007/s13165-019-00275-1, 2020.

Van Genuchten, M. and Alves, W. J.: Analytical Solutions of One Dimensional Convective Dispersive Solute Transport Equations, 1982.

https://doi.org/10.5194/egusphere-2026-3473
Preprint. Discussion started: 21 July 2026

Van Genuchten, M. Th. and Wierenga, P. J.: Mass Transfer Studies in Sorbing Porous Media I. Analytical Solutions, Soil Sci. Soc. Am. J., 40, 473–480, https://doi.org/10.2136/sssaj1976.03615995004000040011x, 1976.

Vaudelet, P., Revil, A., Schmutz, M., Franceschi, M., and Bégassat, P.: Changes in induced polarization associated with the sorption of sodium, lead, and zinc on silica sands, J. Colloid Interface Sci., 360, 739–752, https://doi.org/10.1016/J.JCIS.2011.04.077, 2011.

Vinegar, H. J. and Waxman, M. H.: Induced polarization of shaly sands, https://doi.org/10.1190/1.1441755, 49, 1267–1287, https://doi.org/10.1190/1.1441755, 1984.

de Vries, E. T., Raoof, A., and van Genuchten, M. Th.: Multiscale modelling of dual-porosity porous media; a computational pore-scale study for flow and solute transport, Adv. Water Resour., 105, 82–95, https://doi.org/10.1016/j.advwatres.2017.04.013, 2017.

Warrick, A. W. (Ed.): Soil physics companion, CRC Press, Boca Raton, FL, 389 pp., 2002.

Wuepper, D., Borrelli, P., and Finger, R.: Countries and the global rate of soil erosion, Nat. Sustain., 3, 51–55, https://doi.org/10.1038/s41893-019-0438-4, 2019.

Xuan, K., Li, X., Yu, X., Jiang, Y., Ji, J., Jia, R., Wang, C., and Liu, J.: Effects of different organic amendments on soil pore structure acquired by three-dimensional investigation, Eur. J. Soil Sci., 73, e13264, https://doi.org/10.1111/ejss.13264, 2022.

Yoder, R. E.: A Direct Method of Aggregate Analysis of Soils and a Study of the Physical Nature of Erosion Losses, Agron. J., 28, 337–351, https://doi.org/10.2134/agronj1936.00021962002800050001x, 1936.

Yudina, A. and Kuzyakov, Y.: Dual nature of soil structure: The unity of aggregates and pores, Geoderma, 434, 116478, https://doi.org/10.1016/j.geoderma.2023.116478, 2023.

Zhang, J., Wang, M., Liu, K., and Zhao, Z.: Dynamic changes in soil erosion and challenges to grain productivity in the black soil region of Northeast China, Ecol. Indic., 171, 113145, https://doi.org/10.1016/j.ecolind.2025.113145, 2025.

Zhang, W., Munkholm, L. J., Liu, X., An, T., Xu, Y., Ge, Z., Xie, N., Li, A., Dong, Y., Peng, C., Li, S., and Wang, J.: Soil aggregate microstructure and microbial community structure mediate soil organic carbon accumulation: Evidence from one-year field experiment, Geoderma, 430, 116324, https://doi.org/10.1016/j.geoderma.2023.116324, 2023.

Zhong, X., Li, J., Naveed, M., Raffan, A., and Hallett, P. D.: A laboratory study to disentangle hydrological, mechanical and structural mechanisms of soil stabilization by plant mucilage between eroding and depositional zones of a slope, Eur. J. Soil Sci., 72, 125–140, https://doi.org/10.1111/ejss.12955, 2021.